JOC The Journal of Organic Chemistry

Article

pubs.acs.org/joc

Cp*Co^{III}-Catalyzed C−H Alkenylation/Annulation Reactions of Indoles with Alkynes: A DFT Study

Ken Sakata,*[†,§] Masami Eda,[†] Yuri Kitaoka,[†] Tatsuhiko Yoshino,[‡,§] and Shigeki Matsunaga[‡,§]

[†]Faculty of Pharmaceutical Sciences, Hoshi University, Ebara, Shinagawa-ku, Tokyo 142-8501, Japan

[‡]Faculty of Pharmaceutical Sciences, Hokkaido University, Sapporo 060-0812, Japan

[§]ACT-C, Japan Science and Technology Agency, Sapporo 060-0812, Japan

Supporting Information

ABSTRACT: The Cp*Co^{III}-catalyzed C−H functionalization reaction of indoles with alkynes was examined using M06-level DFT calculations. The C≡C bond in the alkyne was inserted into the Co−C bond of an intermediate alkenyl−Co complex given by the acetate-assisted C−H bond activation step. Then the reaction pathway bifurcated into alkenylation and annulation pathways. In the case where AcOH, which was eliminated by ligand exchange for the alkyne, recoordinated to the Co atom, alkenylation proceeded via proton transfer. On the other hand, the annulation pathway to give pyrroloindolone became significant in the case where the ring-closure C−C bond formation was followed by the attachment of AcOH. At a high temperature (393 K), the difference in the Gibbs free energy between the transition state for proton transfer in the alkenylation pathway and that for the ring-closure C−C bond formation in the annulation pathway was relatively small, so both reactions could proceed. In addition, we also found another pathway to provide the directing-group migration on the way to annulation. This finding well elucidates the recent experimental report that tetrasubstituted alkenes were obtained as the major product under different conditions.

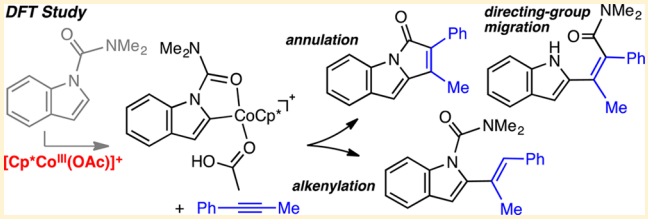

INTRODUCTION

Over the last two decades, there has been considerable interest in transition-metal-catalyzed C−H bond functionalization from the viewpoint of atom and step economy.[1] Among a variety of transition-metal catalysts, cationic Cp*Rh^{III} (Cp* = pentamethylcyclopentadienyl) complexes are known to have high catalytic activity and generality for directing-group-assisted functionalization of aromatic C−H bonds.[2] However, the Rh catalyst suffers from its high cost. To overcoming this weakness, Kanai, Matsunaga, and co-workers recently examined inexpensive Cp*Co^{III} complexes as an alternative to the Cp*Rh^{III} catalyst and revealed the utility of the catalysts for directed C−H bond activation.[3] Since then, Cp*Co^{III} catalysts have been successfully applied to many types of functionalizations.[4−6]

One of the distinct catalytic abilities of cationic Cp*Co^{III} complexes is the reaction of indoles with alkynes (Scheme 1).[4a] While the Cp*Rh^{III} catalyst provides C2-selective alkenylation in the reaction,[7] the Cp*Co^{III} catalyst provides pyrroloindolone as well as the alkenylation product. Some other examples of Cp*Co^{III}-catalyzed annulation reactions have been reported quite recently.[8] According to the proposed catalytic cycle for the annulation reaction (Scheme 2), the C2-selective C−H metalation is followed by the insertion of the alkyne and the subsequent release of the amine. In our previous study, we examined the C−H metalation step using DFT calculations and proposed that the step proceeds via a concerted metalation−deprotonation (CMD) mechanism.[4a,9] Herein we further examine the successive steps for the [Cp*Co^{III}(OAc)]$^+$-catalyzed alkenylation/annulation reaction of indoles (**1**) with alkynes (**2**) using M06-level DFT calculations (Scheme 3). Recenty, Qu and Cramer performed M06-L level DFT study of Cp*Co^{III}-catalyzed C−H bond functionalizations with diazo-compound substrates[6] and found that the singlet-state structures are lower in energy than triplet and quintet-state structures. Our previous study showed that both singlet and triplet pathways are important for the C−H metalation step.[4a] Thus, pathways in closed-shell singlet and triplet states are considered in the present study.

Scheme 1. Cp*Co-Catalyzed C−H Alkenylation/Annulation Reactions (ref 4a)

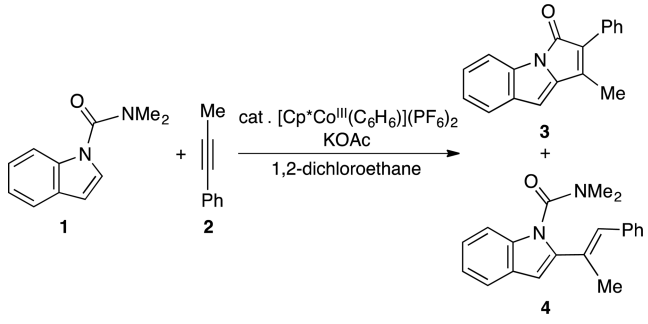

Received: May 1, 2017
Published: July 5, 2017

DOI: 10.1021/acs.joc.7b01047
J. Org. Chem. 2017, 82, 7379−7387

Scheme 2. Proposed Catalytic Cycle (ref 4a)[a]

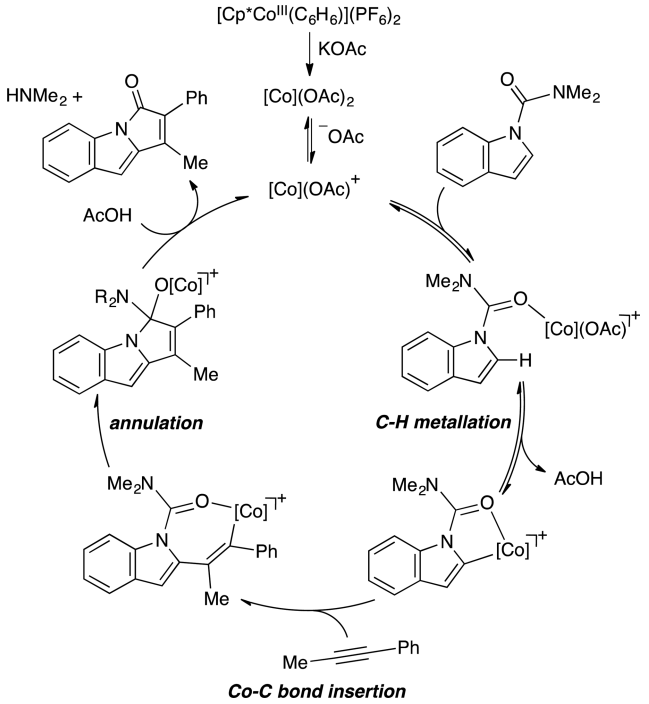

[a][Co] stands for Cp*Co.

Scheme 3. Reaction Pathways Examined in the Present Study[a]

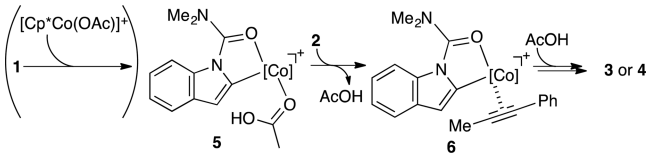

[a][Co] stands for [Cp*Co].

RESULTS AND DISCUSSION

Co−C Bond Insertion. The initial complex $''\mathbf{5}$ (n = 1 for singlet state and n = 3 for triplet state) is given by the acetate-assisted C−H bond activation between indole **1** and the catalyst $[Cp^*Co(OAc)]^+$.[4a] The singlet-state $^1\mathbf{5}$ is lower in Gibbs free energy than the triplet-state $^3\mathbf{5}$ by 5.4 kcal/mol.[10] Ligand exchange between alkyne **2** and AcOH in $''\mathbf{5}$ affords the π-complex $''\mathbf{6}$. Then the C≡C bond in the coordinated alkyne is inserted into the Co−C bond via transition-state, $^1\mathbf{TS}_{6-7}$ or $^3\mathbf{TS}_{6-8}$, to finally give complex $''\mathbf{8}$ or $''\mathbf{9}$. The Gibbs free energy diagrams at 393 K are shown in Figure 1.

In the π-complex $^1\mathbf{6}$ and the transition-state $^1\mathbf{TS}_{6-7}$, the Gibbs free energies at 393 K relative to the initial state ($^1\mathbf{5} + \mathbf{2}$), $\Delta G^{393\ K}$, are 3.3 and 12.8 kcal/mol, respectively.[11] The energy barrier is not so high, so this step easily proceeds. The transition-state $^1\mathbf{TS}_{6-7}$ leads to complex $^1\mathbf{7}$ ($\Delta G^{393\ K}$ = −9.5 kcal/mol), in which the weak interaction between the Co and C atoms remains. This interaction is not present in complex $^1\mathbf{9}$ ($\Delta G^{393\ K}$ = −10.2 kcal/mol) through the pathway of $^1\mathbf{TS}_{7-8}$ ($\Delta G^{393\ K}$ = −5.4 kcal/mol) → $^1\mathbf{8}$ ($\Delta G^{393\ K}$ = −12.7 kcal/mol) → $^1\mathbf{TS}_{8-9}$ ($\Delta G^{393\ K}$ = −6.7 kcal/mol).

In the triplet state, the transition state of the Co−C bond insertion, $^3\mathbf{TS}_{6-8}$, leads to complex $^3\mathbf{8}$, in which there exists no interaction between the Co and C atoms (the distance between the Co and C atoms is 3.00 Å). Complex $^3\mathbf{9}$ has a similar structure as $^3\mathbf{8}$, but the Co atom in $^3\mathbf{9}$ is farther from the indole moiety than that in $^3\mathbf{8}$ (the distance between the Co and C atoms in $^3\mathbf{9}$ is 3.32 Å). The $\Delta G^{393\ K}$ of $^3\mathbf{6}$ and $^3\mathbf{TS}_{6-8}$ are 12.0 and 19.4 kcal/mol, respectively, which are much higher than those of $^1\mathbf{6}$ and $^1\mathbf{TS}_{6-8}$.[12] Thus, the singlet-state pathway is preferred to the triplet pathway in the Co−C insertion step; however, the $\Delta G^{393\ K}$ of $^3\mathbf{8}$ and $^3\mathbf{9}$ are lower than those of the corresponding singlet structures, $^1\mathbf{8}$ and $^1\mathbf{9}$.

Reactivity of Co−C Bond Insertion. Insertions of olefins or alkynes into metal−carbon σ-bonds have been known to be one step in the catalytic cycles for a variety of metal-catalyzed reaction systems.[14,15] To clarify the reactivity of the polarized Co−C bond,[4a] we further examined the singlet transition-state $^1\mathbf{TS}_{6-7}$ of which the structure is shown in Figure 2. The change in the bond lengths along the IRC[16] is shown in Figure 3(a). While the bond length between the Co and C^3 atoms, $r(Co-C^3)$, gradually shortens along the reaction coordinate (s), the length between the C^1 and C^2 atoms, $r(C^1-C^2)$, becomes largely shorter near the transition state (s = 0). The Co−C^1 bond, which is transformed from a σ-type bond ($^1\mathbf{6}$) into a π-coordination bond ($^1\mathbf{7}$), lengthens after the transition state. The change in the Mulliken overlap population[17] for these bonds is shown in Figure 3(b). The population for the Co−C^3 bond shows small variation throughout the course of the reaction.[18] The population for the C^1-C^2 bond is negative (s < 0) and then increases positively near the transition state, while the population for the Co−C^1 bond decreases along the reaction coordinate. The decomposition of the overlap population in terms of fragment MOs shows that the rapid increase in the overlap population for the C^1-C^2 bond depends on the contribution between occupied MOs of the cobalt complex fragment and unoccupied MOs of the alkyne fragment (see Figure S4 in Supporting Information).[21] Thus, the increase of the population is due to back-donation from the cobalt complex to the alkyne.

Alkenylation. In the case where AcOH, which is eliminated by ligand exchange in the Co−C bond-insertion step, recoordinates to the Co atom in $^1\mathbf{9}$, alkenylation proceeds through proton transfer from the coordinated AcOH to the alkenyl carbon atom, as shown in Figure 4 (for the detailed pathway, see Figure S6 in Supporting Information). Formation of the hydrogen-bonded complex $^1\mathbf{10}$ ($\Delta G^{393\ K}$ = −1.2 kcal/mol) and subsequent Co−O bond formation via $^1\mathbf{TS}_{10-11}$ ($\Delta G^{393\ K}$ = 1.5 kcal/mol) gives the AcOH-coordinated complex $^1\mathbf{11}$ ($\Delta G^{393\ K}$ = −6.1 kcal/mol). After the transformation of $^1\mathbf{11}$ into $^1\mathbf{12}$ through hydrogen-bond breaking, proton transfer occurs via $^1\mathbf{TS}_{12-13}$ (Figure 5). The $\Delta G^{393\ K}$ of $^1\mathbf{TS}_{12-13}$ is 7.2 kcal/mol, which is the highest among the alkenylation pathways. Transition-state $^1\mathbf{TS}_{12-13}$ leads to complex $^1\mathbf{13}$, in which interactions exist between the Co atom and the alkenyl C=C bond and between the acetate oxygen atom and the alkenyl hydrogen atom (see Figures S6 and S7 in Supporting Information). Complex $^1\mathbf{13}$ is easily transformed into $^1\mathbf{14}$ and further into $^1\mathbf{15}$ ($\Delta G^{393\ K}$ = −20.7 kcal/mol), where the alkenylation product, **4**, coordinates to the catalyst $[Cp^*Co(OAc)]^+$. In the triplet state, similar pathways were obtained. Thus, the formation of the Co−O coordination bond ($''\mathbf{TS}_{10-11}$) and proton transfer ($''\mathbf{TS}_{12-13}$) are important steps among the alkenylation pathways. In the former step, the triplet pathway is preferred, while the singlet pathway becomes slightly lower in energy in the latter step.

Annulation. It has been experimentally reported that pyrroloindolone is not obtained when treating the alkenyl product under the reaction conditions.[4a] In the alkenylation

DOI: 10.1021/acs.joc.7b01047
J. Org. Chem. 2017, 82, 7379−7387

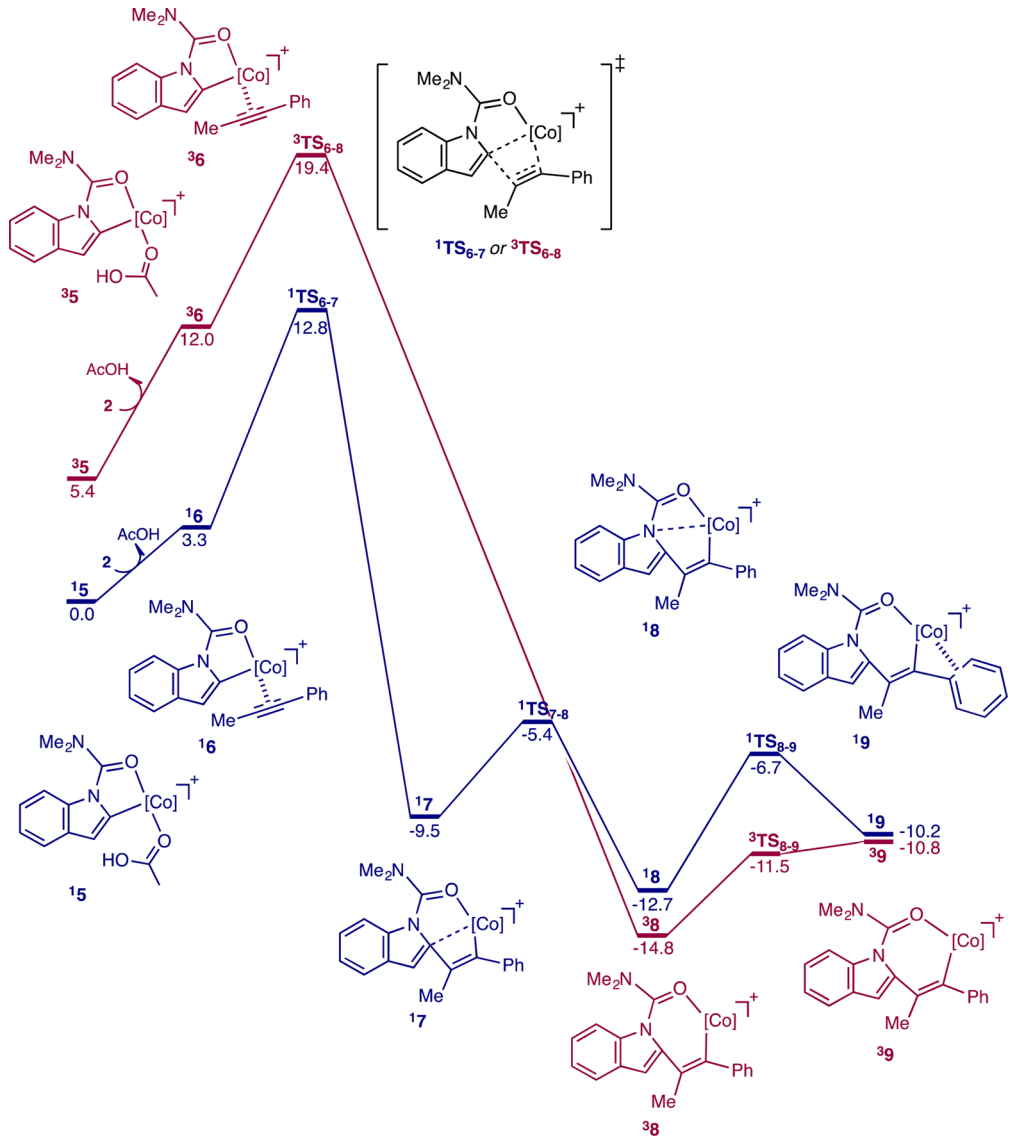

Figure 1. Gibbs free energy ($\Delta G^{393\ K}$) diagrams at 393 K (kcal/mol). [Co] stands for [Cp*Co].

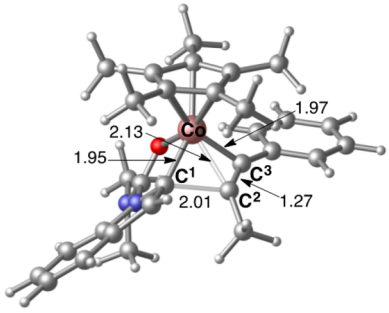

Figure 2. Structure of the singlet transition state for the Co−C bond insertion, ^{1}**TS**$_{6-7}$. Bond lengths are in angstroms (Å).

product complex ″**15**, the carbamoyl carbon atom has a highly positive atomic charge (+0.92 and +0.91 in ^{1}**15** and ^{3}**15**, respectively, by natural population analysis[22]), indicating the high electrophilicity of the carbamoyl carbon. The attack of the alkenyl carbon to the carbamoyl carbon affords complex ″**41** through ″**TS**$_{15-41}$. Then, the transformation of ″**41** to the different conformer ″**42** and the subsequent elimination of dimethylamine gives the pyrroloindolone-[Cp*Co(OAc)]$^{+}$ complex ″**26** (Figure 6). However, the energy barrier from ^{1}**15** to ^{1}**TS**$_{15-41}$ was calculated to be 39.8 kcal/mol, which is quite large. In the triplet state, the barrier from ^{3}**15** to ^{3}**TS**$_{15-41}$ is also large (35.9 kcal/mol); however, the $\Delta G^{393\ K}$ of ^{3}**TS**$_{15-41}$ is lower than that of ^{1}**TS**$_{15-41}$. These results show that the direct transformation pathway from **15** to **26** is not significant, as suggested by experimental results.

Thus, we examined other annulation pathways for the nucleophilic attack of the Co-bonded alkenyl carbon atom to the carbamoyl carbon atom, i.e., the ring-closure C−C bond formation, after the formation of complex ″**9** in the Co−C insertion step. Three types of pathways (paths A, B, and C) for the ring-closure C−C bond formation were considered (Figure 7). In path A, the C−C bond is formed without AcOH. The singlet transition state of the C−C bond formation along path A corresponds to ^{1}**TS**$_{9-16}$ ($\Delta G^{393\ K}$ = 8.8 kcal/mol), which connects complex ^{1}**9** to complex ^{1}**16** (Figure 8). In these structures, the phenyl group weakly interacts with the Co atom. The $\Delta G^{393\ K}$ of the triplet transition-state ^{3}**TS**$_{9-16}$ is 9.2 kcal/mol, which is almost the same as that of the singlet state. Through umbrella inversion around the carbamoyl nitrogen atom,

DOI: 10.1021/acs.joc.7b01047
J. Org. Chem. 2017, 82, 7379−7387

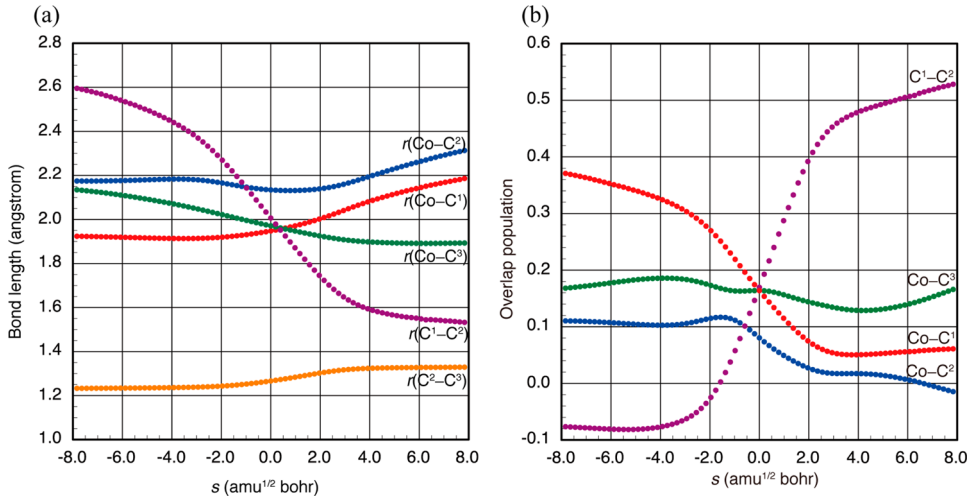

Figure 3. Changes in (a) bond lengths and (b) Mulliken overlap populations along the IRC of ^{1}**TS**$_{6-7}$.

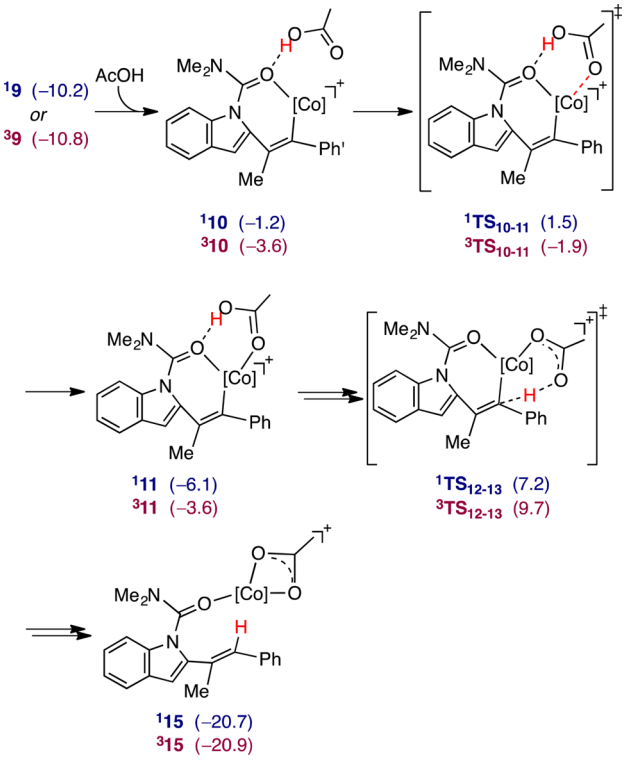

Figure 4. Alkenylation pathway. Relative free energies $\Delta G^{393\ K}$ (kcal/mol) are in parentheses. [Co] stands for [Cp*Co]. The phenyl group represented by Ph′ interacts with the Co atom in the singlet state.

complex ^{1}**16** is easily transformed to complex ^{1}**17**. Then, ^{1}**17** interacts with AcOH through a hydrogen bond to give complex ^{1}**19**, and the formation of the Co−O bond provides complex ^{1}**20** via ^{1}**TS**$_{19-20}$. The $\Delta G^{393\ K}$ of ^{1}**TS**$_{19-20}$ is 10.6 kcal/mol, which is higher than that of ^{1}**TS**$_{9-16}$. On the other hand, the $\Delta G^{393\ K}$ of the corresponding triplet transition-state ^{3}**TS**$_{19-20}$ is 7.1 kcal/mol, which is lower than that of ^{1}**TS**$_{19-20}$. Therefore, the triplet pathway is preferred to the singlet pathway after the Co−C bond formation step (see Figure S11 in Supporting Information for the detailed energy diagram).

In path B, the C−C bond formation proceeds in the presence of AcOH. Specifically, the hydrogen-bonded complex ^{1}**10** is transformed to complex ^{1}**18** via transition-state ^{1}**TS**$_{10-18}$. The

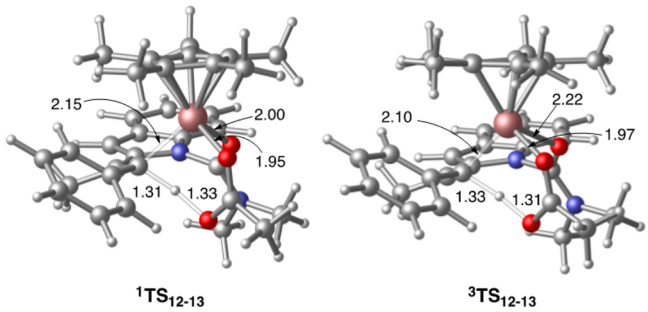

^{1}**TS**$_{12-13}$ ^{3}**TS**$_{12-13}$

Figure 5. Transition-state structures for proton transfer, ^{1}**TS**$_{12-13}$ and ^{3}**TS**$_{12-13}$. Bond lengths are in angstroms (Å).

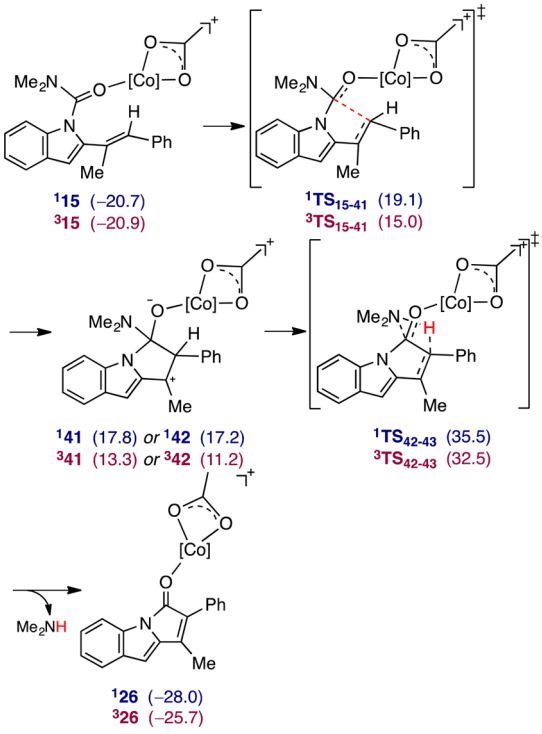

Figure 6. Direct transformation from the alkenylation product complex **15** to the annulation product complex 26. Relative free energies $\Delta G^{393\ K}$ (kcal/mol) are in parentheses. [Co] stands for [Cp*Co].

DOI: 10.1021/acs.joc.7b01047
J. Org. Chem. 2017, 82, 7379−7387

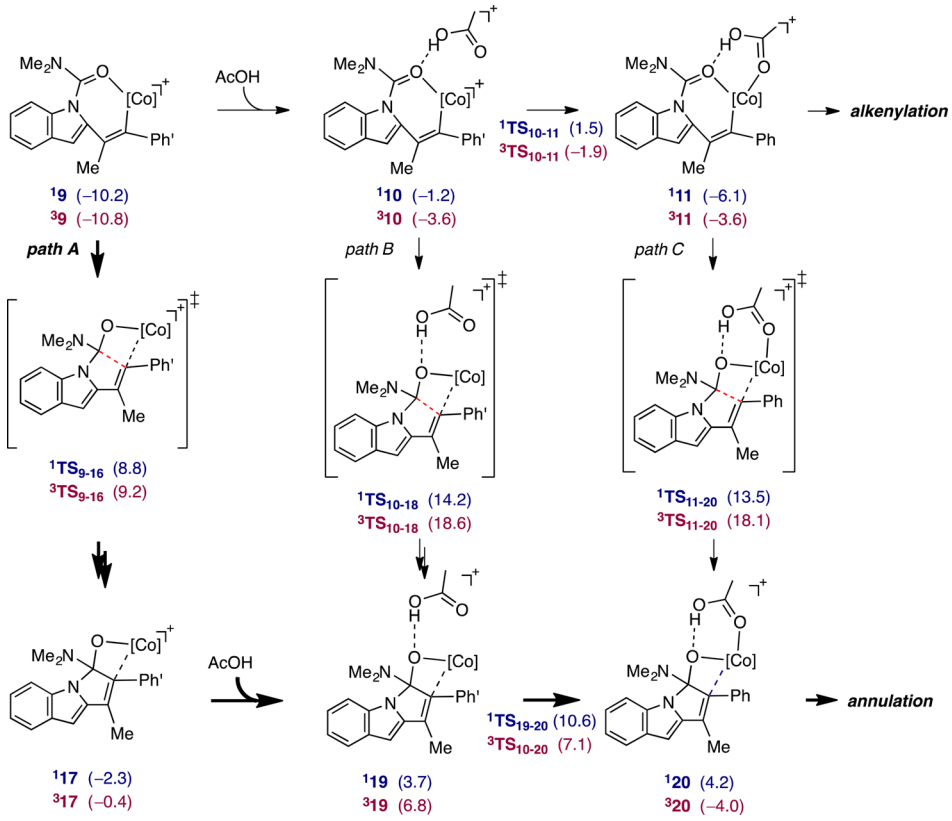

Figure 7. Three types of transition states for the ring-closure C−C bond formation. Relative free energies $\Delta G^{393\ K}$ (kcal/mol) are in parentheses. [Co] stands for [Cp*Co]. The phenyl group represented by Ph′ interacts with the Co atom in the singlet state. There is no interaction between Co atom and the alkyne C atom in triplet-state complex ^{3}20, while the interaction exists in singlet-state complex ^{1}**20**.

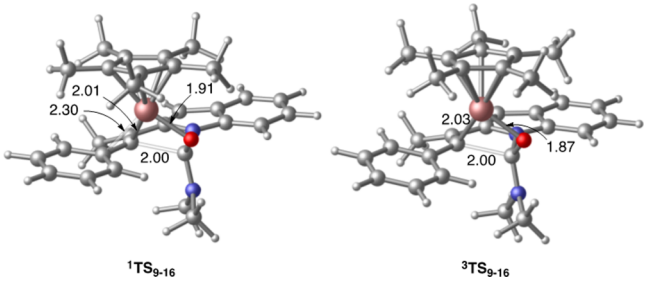

Figure 8. Transition-state structures for the C−C bond formation, ^{1}**TS**$_{9-16}$ and ^{3}**TS**$_{9-16}$. Bond lengths are in angstroms (Å).

$\Delta G^{393\ K}$ of ^{1}**TS**$_{10-18}$ is 14.2 kcal/mol, which is much higher than that of ^{1}**TS**$_{9-16}$ (path A). The $\Delta G^{393\ K}$ of the corresponding triplet transition-state ^{3}**TS**$_{10-18}$ is also higher (18.6 kcal/mol). Thus, path B is not favored. In path C, the Co−C bond formation is followed by C−C bond formation. Complex ^{n}**11** is transformed to complex ^{n}**20** via transition-state ^{n}**TS**$_{11-20}$. The $\Delta G^{393\ K}$ of ^{1}**TS**$_{11-20}$ and ^{3}**TS**$_{11-20}$ are 13.5 and 18.1 kcal/mol, respectively, which are also higher than those of ^{1}**TS**$_{9-16}$.[23] On the basis of these results, path A, in which the C−C bond formation is followed by AcOH coordination, is preferred to the other two pathways (paths B and C).

The triplet-state complex ^{3}**20** ($\Delta G^{393\ K}$ = −4.0 kcal/mol) given through path A is much lower in free energy than the singlet-state structure ^{1}**20** ($\Delta G^{393\ K}$ = 4.2 kcal/mol). As shown in Figure 9, ^{3}**20** is easily transformed to the pyrroloindolone-[Cp*Co(OAc)]$^+$ complex ^{3}**26** through hydrogen-bond exchange between the N and O atoms (^{3}**20** → ^{3}**TS**$_{20-21}$ →^{3}**21**), proton transfer (^{3}**21** → ^{3}**TS**$_{21-22}$ →^{3}**22**), coordination of the other acetate oxygen atom to the Co atom (^{3}**22** → ^{3}**TS**$_{22-23}$ → ^{3}**23**), and elimination of dimethylamine (^{3}**23** → ^{3}**TS**$_{23-24}$ → ^{3}**24** → ^{3}**26**) (see Figure S13 in Supporting Information for the detailed energy diagram). When AcOH immediately coordinates to the Co atom after the ring-closure C−C bond formation (^{1}**TS**$_{9-16}$ or ^{3}**TS**$_{9-16}$), the annulation reaction readily proceeds utilizing the triplet-state pathway.

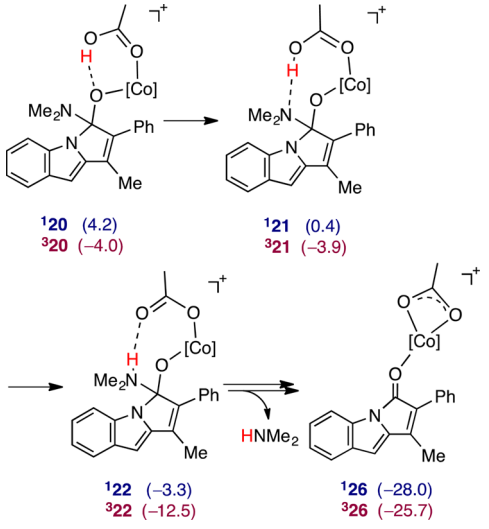

Figure 9. Annulation pathway after the ring-closure C−C bond formation. Relative free energies $\Delta G^{393\ K}$ (kcal/mol) are in parentheses. Triplet-state structures are shown (see Figure S13 for singlet state). [Co] stands for [Cp*Co].

DOI: 10.1021/acs.joc.7b01047
J. Org. Chem. 2017, 82, 7379−7387

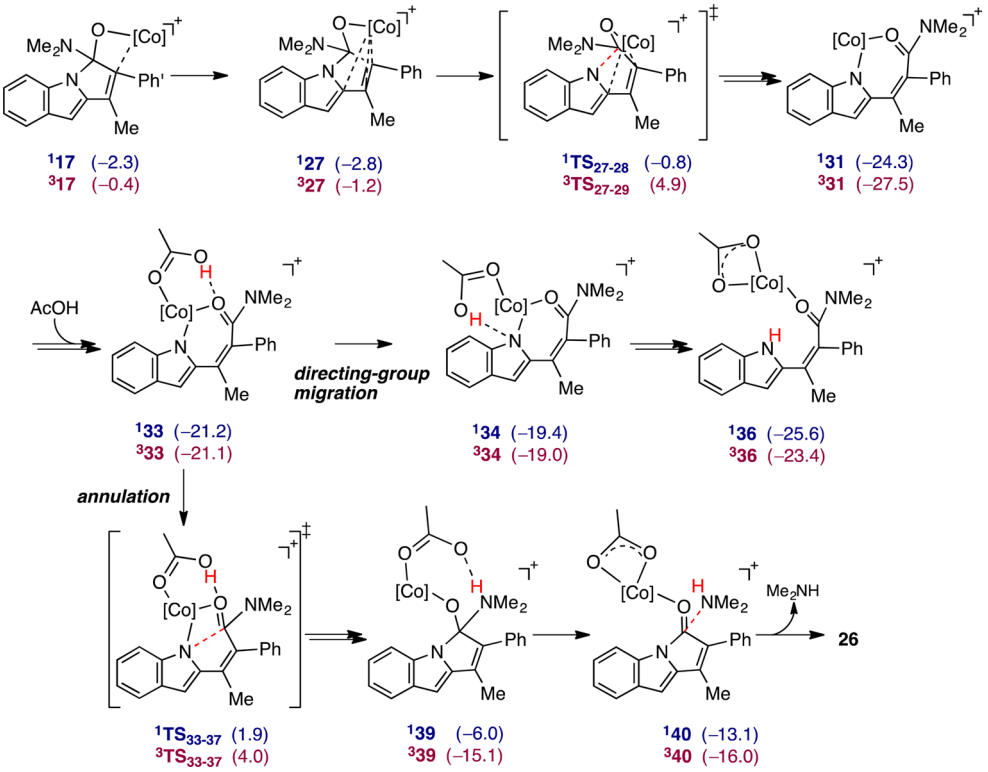

Figure 10. Directing-group migration pathway to give tetrasubstituted alkenes. Relative free energies $\Delta G^{393\ K}$ (kcal/mol) are in parentheses. [Co] stands for [Cp*Co]. The phenyl group represented by Ph′ interacts with the Co atom in the singlet state.

Directing-Group Migration. For the pathway following the ring-closure C−C bond formation step in the annulation pathway, another pathway involving directing-group migration was also found (Figure 10; see Figures S14−S17 in Supporting Information for detailed results).[24,25] In the absence of AcOH, complex ^{1}**17**, which is given through the ring-closure C−C bond formation step via ^{1}**TS**$_{9-16}$, is easily transformed to complex ^{1}**27** ($\Delta G^{393\ K}$ = −2.8 kcal/mol), in which the Co atom coordinates to both the alkyne carbon atoms and the C2 atom in the indole, via ^{1}**TS**$_{16-27}$ ($\Delta G^{393\ K}$ = 0.3 kcal/mol). Then the bond between the nitrogen atom in the indole and the carbamoyl carbon atom is cleaved to give complex ^{1}**30** ($\Delta G^{393\ K}$ = −22.8 kcal/mol) or ^{1}**31** ($\Delta G^{393\ K}$ = −24.3 kcal/mol), which are much lower in free energy through this pathway (^{1}**TS**$_{27-28}$ ($\Delta G^{393\ K}$ = −0.8 kcal/mol) → ^{1}**28** ($\Delta G^{393\ K}$ = −12.8 kcal/mol) → ^{1}**TS**$_{28-29}$ ($\Delta G^{393\ K}$ = −8.5 kcal/mol) → ^{1}**29** ($\Delta G^{393\ K}$ = −10.8 kcal/mol) → ^{1}**TS**$_{29-30}$ ($\Delta G^{393\ K}$ = −7.0 kcal/mol) → ^{1}**30**). The triplet-state pathway is also obtained, and the $\Delta G^{393\ K}$ of these triplet-state structures are even lower ($\Delta G^{393\ K}$ = −27.0 and −27.5 kcal/mol for ^{3}**30** and ^{3}**31**, respectively).

The coordination of AcOH to ″**31** gives the complex ″**33** via the hydrogen-bonded complex ″**32** and transition-state ″**TS**$_{32-33}$. Complex ″**33** is easily transformed to the tetrasubstituted alkene-[Cp*Co(OAc)]$^+$ complex ″**36** along the pathway that involves proton transfer (″**33** → ″**TS**$_{33-34}$ → ″**34** → ″**TS**$_{34-35}$ → ″**35**) and coordination of the other acetate oxygen atom to the Co atom (″**35** → ″**TS**$_{35-36}$ → ″**36**). On the other hand, the pyrroloindolone-[Cp*Co(OAc)]$^+$ complex ″**26** is also given through the pathway that bifurcates from ″**33** (^{1}**33** → ^{1}**TS**$_{33-37}$ → ^{1}**37** → ^{1}**TS**$_{37-38}$ → ^{1}**38** → ^{1}**TS**$_{38-39}$ → ^{1}**39** → ^{1}**TS**$_{39-40}$ → ^{1}**40** → ^{1}**TS**$_{40-26}$ → ^{1}**26** in the singlet state and ^{3}**33** → ^{3}**TS**$_{33-37}$ → ^{3}**37** → ^{3}**TS**$_{37-39}$ → ^{3}**39** → ^{3}**TS**$_{39-40}$ → ^{3}**40** → ^{3}**TS**$_{40-26}$ → ^{3}**26** in the triplet state). The $\Delta G^{393\ K}$ of ^{1}**TS**$_{33-37}$ and ^{3}**TS**$_{33-37}$ were calculated to be 1.9 and 4.0 kcal/mol, respectively, and the reaction barriers from ″**33** are relatively high (23.1 and 25.1 kcal/mol in the singlet and triplet states, respectively). In the absence of immediate proton transfer after the ring-closure C−C bond formation, the directing-group migration pathway becomes dominant. Quite recently, Matsunaga, Yoshino, and co-workers reported α,β-unsaturated amides as the major products in this reaction system.[4e]

Comparison between the Alkenylation and Annulation Pathways. Now we discuss the comparison between the alkenylation and annulation pathways. Both reaction pathways proceed through the same route until the formation of complex ″**8** or ″**9**. Then alkenylation proceeds via proton transfer (^{1}**TS**$_{12-13}$ or ^{3}**TS**$_{12-13}$) when AcOH attacks ″**9** (left-side pathway from ″**8** in Figure 11). On the other hand, annulation occurs when the ring-closure C−C bond formation (″**TS**$_{9-16}$) is followed by the coordination of AcOH (right-side pathway from ″**8** in Figure 11).

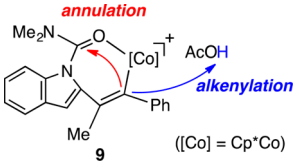

At 393 K, the difference in Gibbs free energy between ″**TS**$_{12-13}$ (7.2 kcal/mol for ^{1}**TS**$_{12-13}$ and 9.7 kcal/mol for ^{3}**TS**$_{12-13}$) and ″**TS**$_{9-16}$ (8.8 kcal/mol for ^{1}**TS**$_{9-16}$ and 9.2 kcal/mol for ^{3}**TS**$_{9-16}$) is relatively small. Therefore, two reactions proceed competitively; however, the alkenylation step is marginally preferred to the annulation step. Both **3** and **4** were experimentally obtained as products.[4a] For the *N*-carbamoylindole bearing a morpholine unit, the transition state corresponding to ^{1}**TS**$_{9-16}$, ^{1}**TS′**$_{9-16}$, is

DOI: 10.1021/acs.joc.7b01047
J. Org. Chem. 2017, 82, 7379−7387

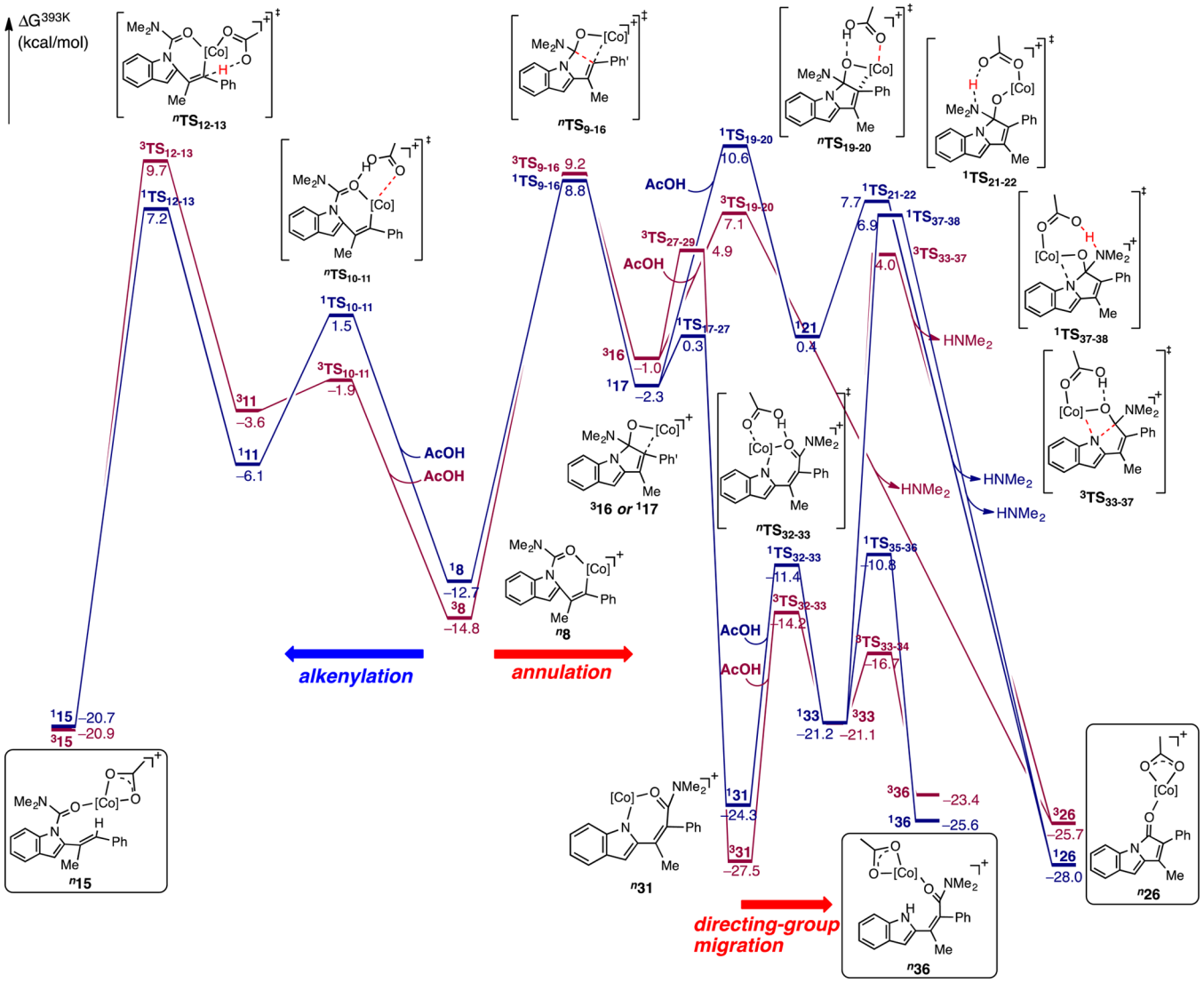

Figure 11. Summarized Gibbs free energy ($\Delta G^{393\ K}$) diagrams at 393 K (kcal/mol) after the Co−C bond-insertion step. Important complexes and transition states are represented in this diagram (for detailed free energy diagrams, see Figures S7, S11, S13, and S17 in Supporting Information). [Co] stands for [Cp*Co]. The phenyl group represented by Ph′ interacts with the Co atom in the singlet state.

lower in free energy at 393 K than those corresponding to ^{1}**TS**$_{12-13}$ and ^{3}**TS**$_{12-13}$, ^{1}**TS′**$_{12-13}$ and ^{3}**TS′**$_{12-13}$, by 1.9 kcal/mol (see Figure S19 in Supporting Information).

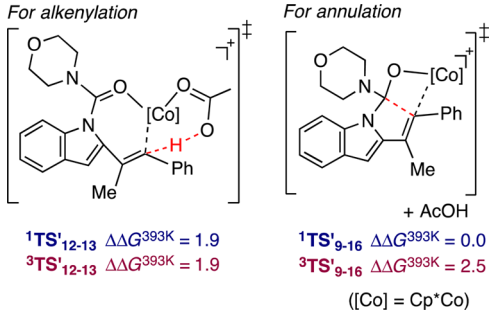

The experimental results certainly show that annulation is preferred to alkenylation in the case of the morpholine group.[4a] These results are in qualitative agreement with the experimental results.[26]

On the other hand, the $\Delta G^{353\ K}$ of the former transition state (4.8 kcal/mol for ^{1}**TS**$_{12-13}$) is much lower than that of the latter transition state (7.9 kcal/mol for ^{1}**TS**$_{9-16}$) at a lower temperature of 353 K. In this case, alkenylation is much preferred to annulation. The alkenylation product **4** has been reported as the major product at 353 K.[4a]

Comparison between the Annulation and Directing-Group Migration Pathways. After the ring-closure C−C bond formation step in the annulation pathway, immediate AcOH coordination and subsequent proton transfer prompt the formation of the pyrroloindolone complex utilizing the triplet-state pathway. Meanwhile, there is another pathway toward the tetrasubstituted alkene complex (Scheme 4). N−C bond cleavage before AcOH coordination, ^{3}**16** or ^{1}**17** → ^{n}**31** in Figure 11, easily gives the tetrasubstituted alkene complex ^{n}**36**. In recent experiments, the tetrasubstituted alkene was observed to be a major product at 373 K.[4e] This result agrees with our present results.[28] Moreover, it was experimentally confirmed that the tetrasubstituted alkene obtained at 373 K was transformed to pyrroloindolone at a higher temperature, 403 K, in the presence of the catalyst. The tetrasubstituted alkene complex ^{n}**36** is transformed to the pyrroloindolone complex ^{n}**26**, which is slightly lower in free energy than ^{n}**36**, via the backward route to

DOI: 10.1021/acs.joc.7b01047
J. Org. Chem. 2017, 82, 7379−7387

Scheme 4. Reaction Pathways[a]

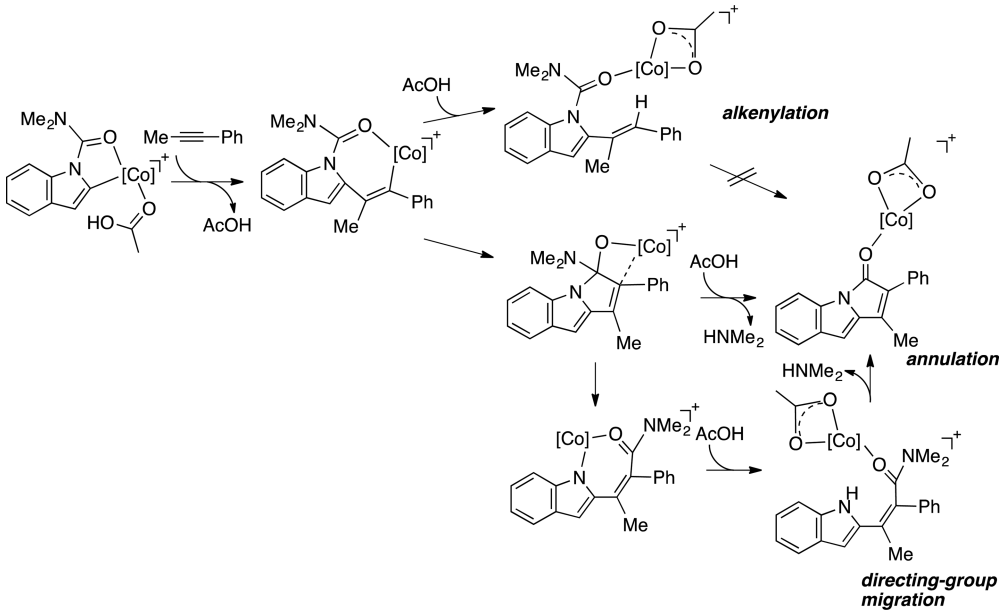

[a][Co] stands for [Cp*Co].

"33; however, there is a slightly high energy barrier for the transformation (^{1}**TS**$_{37-38}$ in the singlet state and ^{3}**TS**$_{33-37}$ in the triplet state). Thus, pyrroloindolone is shown to be thermodynamically preferred to the tetrasubstituted alkene. The pathway through the directing-group migration also plays an important role for the annulation reaction.

CONCLUSION

We examined the C2-selective C−H functionalization reaction of indoles with alkynes catalyzed by a Cp*Co^{III} complex using M06-level DFT calculations. After the insertion of the C≡C bond in the alkyne to the Co−C bond at the alkenyl−Co complex, the alkenylation proceeds by AcOH coordination to the Co atom. On the other hand, the annulation pathway proceeds through the ring-closure C−C bond formation followed by the attachment of AcOH. At a high temperature (393 K), the Gibbs free energies of these transition states are approximately the same, so both pathways are significant. On the other hand, the free energies of the transition states for the alkenylation pathway are lower than those for the annulation pathway at a lower temperature (353 K). Thus, the alkenylation pathway becomes dominant at lower temperature. These results agree with past experimental results. In addition, we also found the directing-group migration pathway to give the tetrasubstituted alkene to occur along the annulation pathway. This pathway plays crucial roles for generating pyrroloindolone as well as the tetrasubstituted alkene. This finding well elucidates the experimental results reported recently by Matsunaga, Yoshino, and co-workers.

EXPERIMENTAL SECTION

Computational Details. DFT calculations were carried out with the Gaussian09[29] program package. Geometry optimization and analytical vibrational frequency analysis were performed by the restricted and unrestricted Kohn−Sham DFT method with the M06 functional.[30] M06 functional is suited for organometallic and main-group chemical systems and for noncovalent interactions.[30,31] In the numerical integration, a larger grid (*ultrafinegrid*) was used.[29] Pople's 6-311G** basis set for C, N, O, and H atoms[32] and the (14s9p5d)/[9s5p3d] basis set of Wachters-Hay with s-, p-, and d-type diffuse and f-type polarization functions for the Co atom[33] were used for the Gaussian basis functions (BSI). The solvent effects of 1,2-dichloroethane were estimated by the CPCM polarizable conductor calculation model[34,35] for the gas-phase optimized structures. For the CPCM calculations, the 6-311++G** basis set for C, N, O, and H atoms (BSII) were used (M06(CPCM)/BSII//M06/BSI).[32,33] The Gibbs free energy at 393 K was estimated by the PCM total energy and the gas-phase thermal free energy.

ASSOCIATED CONTENT

Supporting Information

The Supporting Information is available free of charge on the ACS Publications website at DOI: 10.1021/acs.joc.7b01047.

Tables listing energies and geometries and figures of the free energy diagrams. (PDF)

AUTHOR INFORMATION

Corresponding Author

*E-mail: sakata@hoshi.ac.jp.

ORCID

Ken Sakata: 0000-0002-6920-0735

Notes

The authors declare no competing financial interest.

ACKNOWLEDGMENTS

This work was supported by the JST ACT-C grant number JPMJCR12Z and JSPS KAKENHI grant number JP17K05795, Japan. Some of the calculations were made at the Research Center for Computational Science, Okazaki, Japan. K.S. is grateful to the Research Center for Computational Science for generous permission to use its computing facilities.

REFERENCES

(1) (a) *Transition Metal-Catalyzed Heterocycle Synthesis via C−H Activation*; Wu, X.-F., Ed.; Wiley-VCH: Weinheim, 2016. (b) Rouquet, G.; Chatani, N. *Angew. Chem., Int. Ed.* **2013**, *52*, 11726−11743. (c) Wencel-Delord, J.; Glorius, F. *Nat. Chem.* **2013**, *5*, 369−375.

DOI: 10.1021/acs.joc.7b01047
J. Org. Chem. 2017, 82, 7379−7387

(2) Satoh, T.; Miura, M. *Chem. - Eur. J.* **2010**, *16*, 11212−11222.
(3) (a) Yoshino, T.; Ikemoto, H.; Matsunaga, S.; Kanai, M. *Angew. Chem., Int. Ed.* **2013**, *52*, 2207−2211. (b) Yoshino, T.; Ikemoto, H.; Matsunaga, S.; Kanai, M. *Chem. - Eur. J.* **2013**, *19*, 9142−9146. (c) Sun, B.; Yoshino, T.; Matsunaga, S.; Kanai, M. *Adv. Synth. Catal.* **2014**, *356*, 1491−1495.
(4) (a) Ikemoto, H.; Yoshino, T.; Sakata, K.; Matsunaga, S.; Kanai, M. *J. Am. Chem. Soc.* **2014**, *136*, 5424−5431. (b) Suzuki, Y.; Sun, B.; Sakata, K.; Yoshino, T.; Matsunaga, S.; Kanai, M. *Angew. Chem., Int. Ed.* **2015**, *54*, 9944−9947. (c) Sun, B.; Yoshino, T.; Kanai, M.; Matsunaga, S. *Angew. Chem., Int. Ed.* **2015**, *54*, 12968−12972. (d) Tanaka, R.; Ikemoto, H.; Kanai, M.; Yoshino, T.; Matsunaga, S. *Org. Lett.* **2016**, *18*, 5732−5735. (e) Ikemoto, H.; Tanaka, R.; Sakata, K.; Kanai, M.; Yoshino, T.; Matsunaga, S. *Angew. Chem., Int. Ed.* **2017**, *56*, 7156−7160.
(5) For reviews, see (a) Moselage, M.; Li, J.; Ackermann, L. *ACS Catal.* **2016**, *6*, 498−525. (b) Usman, M.; Ren, Z.-H.; Wang, Y.-Y.; Guan, Z.-H. *Synthesis* **2017**, *49*, 1419−1443. (c) Wang, S.; Chen, S.-Y.; Yu, X.-Q. *Chem. Commun.* **2017**, *53*, 3165−3180. (d) Yoshino, T.; Matsunaga, S. *Adv. Synth. Catal.* **2017**, *359*, 1245−1262 and references therein..
(6) For recent theoretical study, see: Qu, S.; Cramer, C. J. *J. Org. Chem.* **2017**, *82*, 1195−1204.
(7) Schipper, D. J.; Hutchinson, M.; Fagnou, K. *J. Am. Chem. Soc.* **2010**, *132*, 6910−6911.
(8) (a) Kong, L.; Yu, S.; Zhou, X.; Li, X. *Org. Lett.* **2016**, *18*, 588−591. (b) Lu, Q.; Vásquez-Céspedes, S.; Gensch, T.; Glorius, F. *ACS Catal.* **2016**, *6*, 2352−2356. (c) Yan, Q.; Chen, Z.; Liu, Z.; Zhang, Y. *Org. Chem. Front.* **2016**, *3*, 678−682. (d) Yu, W.; Zhang, W.; Liu, Z.; Zhang, Y. *Chem. Commun.* **2016**, *52*, 6837−6840. (e) Kong, L.; Yang, X.; Zhou, X.; Yu, S.; Li, X. *Org. Chem. Front.* **2016**, *3*, 813−816. (f) Liu, H.; Li, J.; Xiong, M.; Jiang, J.; Wang, J. *J. Org. Chem.* **2016**, *81*, 6093−6099.
(9) For CMD mechanism in C−H activation, see (a) Lapointe, D.; Fagnou, K. *Chem. Lett.* **2010**, *39*, 1119−1126. (b) Ackermann, L. *Chem. Rev.* **2011**, *111*, 1315−1345.
(10) In the triplet state ^{3}**5**, spin densities were localized on the Co atom (+1.92 for the Mulliken spin density).
(11) There are two transition states for the insertion of asymmetrical alkyne **2**. The free energy of the other structure was calculated to be higher by 1.0 kcal/mol. See Figure S3 in Supporting Information.
(12) We confirmed the singlet−triplet energy difference by using the B3LYP* functional which improved in order to estimate the energy splitting between the high-spin and low-spin states (ref 13). The results at the M06 level are consistent with those at the B3LYP* level. See Table S2 in Supporting Information.
(13) (a) Reiher, M.; Salomon, O.; Hess, B. A. *Theor. Chem. Acc.* **2001**, *107*, 48−55. (b) Salomon, O.; Reiher, M.; Hess, B. A. *J. Chem. Phys.* **2002**, *117*, 4729−4737.
(14) Hartwig, J. F. *Organotransition Metal Chemistry from Bonding to Catalysis*; University Science Books: Mill Valley, CA, 2010.
(15) For the theoretical study, see: Thorn, D. L.; Hoffmann, R. *J. Am. Chem. Soc.* **1978**, *100*, 2079−2090.
(16) (a) Fukui, K. *Acc. Chem. Res.* **1981**, *14*, 363−368. (b) Hratchian, H. P.; Schlegel, H. B. *J. Chem. Phys.* **2004**, *120*, 9918−9924.
(17) Mulliken, R. S. *J. Chem. Phys.* **1955**, *23*, 1833−1840 and 1841−1846, 2338−2342, 2343−2346..
(18) The Mayer bond orders (ref 19) along IRC show the same tendencies as the overlap populations except for the Co−C^3 bond (see Figure S5 in Supporting Information). The bond order between Co and C^3 atoms increases gradually along the IRC. For the population analysis along IRC, see ref 20.
(19) Mayer, I. *Chem. Phys. Lett.* **1983**, *97*, 270−274.
(20) Sakata, K. *J. Phys. Chem. A* **2000**, *104*, 10001−10008.
(21) This decomposition method was used in order to estimate the antibonding overlap population between two fragments in the Diels−Alder reaction. See: Sakata, S.; Fujimoto, H. *J. Org. Chem.* **2013**, *78*, 3095−3103.
(22) Reed, A. E.; Curtis, L. A.; Weinhold, F. *Chem. Rev.* **1988**, *88*, 899−926.
(23) We also examined the transition state where the hydrogen atom in AcOH interacts with the carbamyl N atom instead of the O atom, ^{1}**TS**$_{11-20}$′ and/or ^{3}**TS**$_{11-20}$′. The ΔG^{393K} values of the transition states in the singlet and triplet states are 20.6 and 23.3 kcal/mol, respectively, which are higher than those of ^{1}**TS**$_{11-20}$ and/or ^{3}**TS**$_{11-20}$.
(24) Lerchen, A.; Knecht, T.; Daniliuc, C. G.; Glorius, F. *Angew. Chem., Int. Ed.* **2016**, *55*, 15166−15170.
(25) The free energy barrier for the direct transformation from **36** to **26** is high. See Figure S18 in Supporting Information.
(26) AcOH is coordinated to the Co complex in ^{n}**TS**$_{12-13}$, while AcOH is detached from the Co complex in ^{n}**TS**$_{9-16}$. Thus, the entropy effect is important for the comparison between two transition states. In the present study, the entropy term of the Gibbs free energy was estimated by using gas-phase results. The exact estimation of entropy terms in condensed phase is an open question (see ref 27).
(27) (a) Mammen, M.; Shakhnovich, E. I.; Deutch, J. M.; Whitesides, G. M. *J. Org. Chem.* **1998**, *63*, 3821−3830. (b) Ohnishi, Y.; Nakao, Y.; Sato, H.; Nakao, Y.; Hiyama, T.; Sakaki, S. *Organometallics* **2009**, *28*, 2583−2594. (c) Nakai, H.; Ishikawa, A. *J. Chem. Phys.* **2014**, *141*, 174106-1−174106-9.
(28) At 373 K, the ΔG^{393K} value for ^{1}**TS**$_{9-16}$ is higher than that for ^{1}**TS**$_{12-13}$ by 2.3 kcal/mol, while the energy of ^{1}**TS**$_{9-16}$′ is lower than that of ^{1}**TS**$_{12-13}$′ by 1.5 kcal/mol. In the case of *N*-carbamoylindole bearing a morpholine unit, the alkenylation pathway is still disfavored at 373 K.
(29) Frisch, M. J.; Trucks, G. W.; Schlegel, H. B.; Scuseria, G. E.; Robb, M. A.; Cheeseman, J. R.; Scalmani, G.; Barone, V.; Mennucci, B.; Petersson, G. A.; Nakatsuji, H.; Caricato, M.; Li, X.; Hratchian, H. P.; Izmaylov, A. F.; Bloino, J.; Zheng, G.; Sonnenberg, J. L.; Hada, M.; Ehara, M.; Toyota, K.; Fukuda, R.; Hasegawa, J.; Ishida, M.; Nakajima, T.; Honda, Y.; Kitao, O.; Nakai, H.; Vreven, T.; Montgomery, Jr., J. A.; Peralta, J. E.; Ogliaro, F.; Bearpark, M.; Heyd, J. J.; Brothers, E.; Kudin, K. N.; Staroverov, V. N.; Kobayashi, R.; Normand, J.; Raghavachari, K.; Rendell, A.; Burant, J. C.; Iyengar, S. S.; Tomasi, J.; Cossi, M.; Rega, N.; Millam, J. M.; Klene, M.; Knox, J. E.; Cross, J. B.; Bakken, V.; Adamo, C.; Jaramillo, J.; Gomperts, R.; Stratmann, R. E.; Yazyev, O.; Austin, A. J.; Cammi, R.; Pomelli, C.; Ochterski, J. W.; Martin, R. L.; Morokuma, K.; Zakrzewski, V. G.; Voth, G. A.; Salvador, P.; Dannenberg, J. J.; Dapprich, S.; Daniels, A. D.; Farkas, Ö.; Foresman, J. B.; Ortiz, J. V.; Cioslowski, J.; Fox, D. J. *Gaussian 09*, Revision D.01; Gaussian, Inc.: Wallingford, CT, 2009.
(30) Zhao, Y.; Truhlar, D. G. *Theor. Chem. Acc.* **2008**, *120*, 215−241.
(31) Zhao, Y.; Truhlar, D. G. *Acc. Chem. Res.* **2008**, *41*, 157−167.
(32) Hehre, W. J.; Radom, L.; Schleyer, P. v. R.; Pople, J. A. *Ab Initio Molecular Orbital Theory*; Wiley: New York, 1986.
(33) (a) Wachters, A. J. H. *J. Chem. Phys.* **1970**, *52*, 1033−1036. (b) Hay, P. J. *J. Chem. Phys.* **1977**, *66*, 4377−4384. (c) Raghavachari, K.; Trucks, G. W. *J. Chem. Phys.* **1989**, *91*, 1062−1065.
(34) (a) Barone, V.; Cossi, M. *J. Phys. Chem. A* **1998**, *102*, 1995−2001. (b) Cossi, M.; Rega, N.; Scalmani, G.; Barone, V. *J. Comput. Chem.* **2003**, *24*, 669−681.
(35) The CPCM model, in which the conductor-like screening model (COSMO) was applied to the PCM model, is simpler than other sophisticated models such as IEF-PCM. For the comprehensive comparison of IEF-PCM with COSMO, see ref 36.
(36) Klamt, A.; Moya, C.; Palomar, J. *J. Chem. Theory Comput.* **2015**, *11*, 4220−4225.

DOI: 10.1021/acs.joc.7b01047
J. Org. Chem. 2017, 82, 7379−7387